

REPORT DOCUMENTATION PAGE

1a. REPORT SECURITY CLASSIFICATION unclassified		1b. RESTRICTIVE MARKINGS	
2a. SECURITY CLASSIFICATION AUTHORITY		3. DISTRIBUTION/AVAILABILITY OF REPORT	
2b. DECLASSIFICATION/DOWNGRADING SCHEDULE		unlimited	
4. PERFORMING ORGANIZATION REPORT NUMBER(S) MM 5488-86-19		5. MONITORING ORGANIZATION REPORT NUMBER(S)	
6a. NAME OF PERFORMING ORGANIZATION Mechanics & Materials Ctr. Texas A&M University	6b. OFFICE SYMBOL (If applicable)	7a. NAME OF MONITORING ORGANIZATION ONR	
6c. ADDRESS (City, State and ZIP Code) College Station, Texas 77843		7b. ADDRESS (City, State and ZIP Code)	
8a. NAME OF FUNDING/SPONSORING ORGANIZATION ONR	8b. OFFICE SYMBOL (If applicable)	9. PROCUREMENT INSTRUMENT IDENTIFICATION NUMBER Contract N00014-86-K-0298	
8c. ADDRESS (City, State and ZIP Code) Mechanics Division Office of Naval Research/Code 1513A:DLU 800 N. Quincy Street Arlington, VA 22217 - 5000		10. SOURCE OF FUNDING NOS.	
11. TITLE (Include Security Classification) The Dynamic Energy Release Rate for Two Parallel Steadily Propagating Mode III Cracks in a Viscoelastic Body		PROGRAM ELEMENT NO.	PROJECT NO.
		TASK NO.	WORK UNIT NO. 4324-520
12. PERSONAL AUTHOR(S) L. Schovanec and J.R. Walton			
13a. TYPE OF REPORT Technical	13b. TIME COVERED FROM _____ TO _____	14. DATE OF REPORT (Yr., Mo., Day) September 1986	15. PAGE COUNT 29
16. SUPPLEMENTARY NOTATION			
17. COSATI CODES		18. SUBJECT TERMS (Continue on reverse if necessary and identify by block number)	
FIELD	GROUP	SUB. GR.	viscoelasticity dynamic fracture dynamic energy release rate
			Barenblatt zone crack growth
19. ABSTRACT (Continue on reverse if necessary and identify by block number) The dynamic steady-state propagation of two parallel semi-infinite, mode III cracks is considered for a general, infinite, homogeneous, and isotropic linearly viscoelastic body. A Barenblatt type failure zone is introduced in order to cancel the singular stress and a formula for the energy release rate is derived which provides immediate comparisons with the corresponding single crack problem. The influence of crack speed, crack separation, and material properties upon the energy release rate are illustrated with numerical calculations for both power-law material and a standard linear solid.			
20. DISTRIBUTION/AVAILABILITY OF ABSTRACT UNCLASSIFIED/UNLIMITED <input checked="" type="checkbox"/> SAME AS RPT. <input type="checkbox"/> DTIC USERS <input type="checkbox"/>		21. ABSTRACT SECURITY CLASSIFICATION unclassified	
22a. NAME OF RESPONSIBLE INDIVIDUAL Dr. Richard L. Miller, Code 1132P		22b. TELEPHONE NUMBER (Include Area Code) (202) 696-4405	22c. OFFICE SYMBOL

The Dynamic Energy Release Rate for Two Parallel
Steadily Propagating Mode III Cracks in a Viscoelastic Body

by

L. Schovanec* and J. R. Walton**

Department of Mathematics
Texas A&M University
College Station, TX 77840 USA

* Permanent Address: Department of Mathematics, Texas Tech University,
Lubbock, TX 79409

** Supported by the Office of Naval Research under Contract No.
N00014-86-K-0298



Mechanics and Materials Center
TEXAS A&M UNIVERSITY
College Station, Texas

LIBRARY
RESEARCH REPORTS DIVISION
NAVAL POSTGRADUATE SCHOOL
MONTEREY, CALIFORNIA 93940

THE DYNAMIC ENERGY RELEASE RATE FOR TWO
PARALLEL STEADILY PROPAGATING MODE III
CRACKS IN A VISCOELASTIC BODY

L. SCHOVANEC
AND
J. R. WALTON

OFFICE OF NAVAL RESEARCH
DEPARTMENT OF THE NAVY
CONTRACT N00014-86-K-0298
WORK UNIT 4324-520

MM-5488-86-19

SEPTEMBER 1986

Abstract

The dynamic steady-state propagation of two parallel semi-infinite, mode III cracks is considered for a general, infinite, homogeneous, and isotropic linearly viscoelastic body. A Barenblatt type failure zone is introduced in order to cancel the singular stress and a formula for the energy release rate is derived which provides immediate comparisons with the corresponding single crack problem. The influence of crack speed, crack separation, and material properties upon the energy release rate are illustrated with numerical calculations for both power-law material and a standard linear solid.

1. Introduction

In [1] the problem of the dynamic steady-state propagation of a semi-infinite antiplane shear crack in a linear viscoelastic body was investigated. By considering an over-all energy balance and incorporating a Barenblatt type failure zone at the crack tip, an expression for the rate of energy flux into the crack tip, hereafter referred to as the energy release rate (ERR), was derived in [2]. The primary objective of the latter study was to investigate the implications of using the ERR as a fracture criterion for predicating the speed of dynamically propagating cracks in a viscoelastic material. In particular, a steady-state, dynamic elastic calculation would predict that Mode III cracks move at the glassy shear wave speed. However, experimentally observed cracks rarely propagate faster than 20% of that speed. Amplifying on the elastic calculation further, what one finds is that in steady-state the stress intensity factor (SIF) is a constant independent of crack speed, while the ERR is a monotone increasing function of crack speed tending to infinity at the shear wave speed. Thus, increasing crack speed corresponds to increasing energy flux to the crack tip. One is then led to conclude that the only stable steady-state speed is the shear wave speed.

For viscoelastic material it was found in [1] that the SIF is a monotone decreasing function of crack speed for crack speeds between the equilibrium and glassy shear wave speeds and tends to zero at the glassy wave speed. While for crack speeds less than the equilibrium wave speed, the SIF has the constant elastic value. In [2] it was shown that the ERR has much more complicated behavior and in general does not depend monotonically on crack speed. In particular there are intervals of stable

and unstable crack speeds less than the glassy shear wave speed. Thus viscous effects in the body prevent much of the energy input by the applied loads from reaching the crack tip thereby predicting crack speeds much lower than results from an elastic calculation.

It has been conjectured from experimental evidence* that another mechanism limiting crack speeds in viscoelastic material is the interaction of microcracks around the tip of a macrocrack. As a first step toward investigating this conjecture, the problem of two parallel, semi-infinite Mode III cracks dynamically propagating in steady-state is considered in this paper. As demonstrated below it is found that the energy input into the tip of one crack may be reduced by up to a factor of one-half due to the presence of another crack. The influence of crack interaction is greatly influenced by crack speed, crack separation, and material properties (e.g. stress relaxation time and the ratio of glassy to equilibrium shear wave speeds).

In the next section the relevant boundary value problem is presented and solved by reduction to a Riemann-Hilbert boundary value problem in a manner similar to [1]. Section 3 contains the calculation of the ERR following the method of [2]. The paper concludes with numerical examples in Sections 4 that illustrate the general results of Section 2 and 3.

* Private communication with Professor Wolfgang Knauss.

2. The Boundary Value Problem

The specific boundary value problem to be investigated is that of the steady propagation (to the right) with speed V of two parallel, semi-infinite, anti-plane shear cracks in a general, homogeneous, and isotropic, linearly viscoelastic body. The shear modulus, $\mu(t)$, is assumed only to be a positive, non-increasing, and convex function of time, t . The governing equation of motion for the out of plane displacement, u_3 , is

$$\mu * d\Delta u_3 = \rho u_{3,tt}$$

where Δ is the two-dimensional Laplacian, $\Delta = (\partial^2/\partial x_1^2) + (\partial^2/\partial x_2^2)$, and $\mu * d\epsilon$ denotes the Riemann-Stieltjes convolution

$$\mu * d\epsilon = \int_{-\infty}^t \mu(t - \tau) d\epsilon(\tau).$$

The cracks are assumed to lie in the horizontal planes corresponding to $x_1 = h$ and $x_1 = -h$ with their tips aligned in the plane $x_1 = 0$. If the crack faces are subjected to equal loadings, the problem is anti-symmetric about the plane $y_1 = 0$. With the introduction of the Galilean variables, $x = x_1 - Vt$, $y = x_2$, it then suffices to solve the equation of motion in the half-plane $y > 0$ subject to the boundary conditions

$$\sigma_{23}(x, h^+) = \sigma_{23}(x, h^-), \quad -\infty < x < \infty \quad (1)$$

$$\sigma_{23}(x, h) = \frac{\partial}{\partial y} (\mu * du_3) = f(x), \quad x < 0 \quad (2)$$

$$u_3(x, h^+) = u_3(x, h^-), \quad x > 0 \quad (3)$$

$$u_3(x, 0) = 0, \quad -\infty < x < \infty. \quad (4)$$

The boundary value problem is solved by proceeding as in [1]. The Fourier transform, defined by

$$\hat{f}(p, y) = \int_{-\infty}^{\infty} e^{ipx} f(x, y) dx$$

is applied to the equation of motion resulting in the ordinary differential equation

$$\frac{d^2}{dy^2} \hat{u}_3(p, y) = \gamma^2(p) \hat{u}_3$$

where $\gamma^2(p) = p^2 + ipVp/\hat{\mu}(-Vp)$. The solution of the differential equation is written as

$$\hat{u}_3(p, y) = \begin{cases} A(p)e^{-\gamma y} & y > h \\ B(p)\sinh(\gamma y) & 0 < y < h \end{cases}$$

so that (4) is satisfied and a square root of γ^2 with positive real part is selected to insure the stresses and displacements vanish as $y \rightarrow \infty$.

From (1) it easily follows that

$$A(p) = -B(p)e^{\gamma h} \cosh(\gamma h).$$

Define $u(x) = u_3(x, h^+) - u_3(x, h^-)$ and $\sigma(x) = \sigma_{23}(x, h^-) = \sigma_{23}(x, h^+)$.

Then a simple calculation gives

$$\hat{\sigma}(p) = -(iVp)\hat{\mu}(-Vp)\gamma(p)e^{-\gamma h}\cosh(\gamma h)\hat{u}(p). \quad (5)$$

If the Carson transform $\bar{g}(s)$ of the function $g(t)$ is defined by

$$\bar{g}(s) = g(0) + \int_0^{\infty} e^{-ts} dg(t)$$

and $\gamma_1(p) = [1 - \rho V^2/\bar{\mu}(iVp)]^{1/2}$, (5) may be written as

$$\hat{\sigma}(p) = -i\text{sgn}(p)\bar{\mu}(iVp)\gamma_1(p) \frac{1}{2} (1 + e^{-2h|p|\gamma_1})\hat{u}_1(p). \quad (6)$$

Define

$$G_1(p) = -i\text{sgn}(p)\bar{\mu}(iVp)\gamma_1(p) = \text{sgn}(p)\tilde{G}_1(p),$$

$$G_2(p) = \frac{1}{2} (1 + e^{-2h|p|\gamma_1}) = \frac{1}{2} \tilde{G}_2(p),$$

and $G = G_1 G_2$. From (2) and (3) it then follows that (6) may be viewed as the Riemann-Hilbert problem.

$$F^+(p) = G(p)F^-(p) + g(p) \quad (7)$$

where $F^+(p) = \hat{\sigma}^+$, $F^-(p) = \hat{u}_1^-$, $g(p) = -\hat{\sigma} = -\hat{f}(p)$, and $f^+(x)(f^-(x))$ denotes the restriction of $f(x)$ to $x > 0$ ($x < 0$). Note that as $h \rightarrow 0$, $G \rightarrow G_1$ and (7) is precisely the problem of a single crack solved in [1]. Since the solution of (7) is constructed in a similar manner to [1], only a brief outline of the method of solution is presented here.

To solve (7) first consider the homogeneous problem of finding functions $X^\pm(z)$ analytic for $\text{Im}(z) > 0$ which satisfy the boundary relation

$$X^+(p) = (p)X^-(p). \quad (8)$$

The solution of (8) may be written as $X^\pm = X_1^\pm X_2^\pm$ where $X_1^\pm(p) = i(p)X_i^\pm(p)$, $i = 1, 2$. $X_1^\pm(z)$ is given in [1] and $X_2^\pm = w^\pm X_2^\pm$ where

$$\tilde{X}_2^\pm(z) = \exp [\Gamma^\pm(z)]$$

$$\Gamma^\pm(z) = \frac{1}{2\pi i} \int_{-\infty}^{\infty} \frac{\log(\tilde{G}_2(\tau))}{\tau - z} d\tau, \quad (9)$$

and $w^+(p)/w^-(p) = 1/2$. Though $X_2^\pm(z)$ is not uniquely determined, (7) has a unique solution given by

$$F^\pm(z) = \frac{X_1^\pm(z)\tilde{X}_2^\pm(z)}{2\pi i} \int_{-\infty}^{\infty} \frac{g(\tau)/(X_1^\pm X_2^\pm)(\tau)}{\tau - z} d\tau. \quad (10)$$

Utilizing (10) and some trivial modifications of the methods of [1] it can be shown that the asymptotic expansion of $\sigma_{23}^+(x)$ for x near zero is given by $\sigma_{23}^+(x) \sim K/\sqrt{x}$ where the stress intensity factor K is defined by

$$K = \frac{|\tilde{G}_1(\infty)|^{1/2}}{\sqrt{\pi}} \frac{1}{2\pi} \int_{-\infty}^{\infty} \frac{g(\tau)}{X_1^+(\tau)X_2^+(\tau)} d\tau. \quad (11)$$

In the next section attention is focused upon the calculation of the energy release rate, the primary interest of this paper. For special forms of the crack loadings explicit formulas for the ERR and the SIF are developed. The paper concludes by presenting numerical results for the special cases of a power-law material and a standard linear solid.

3. The Energy Release Rate

As discussed in [2], the energy flux into the tip of an extending crack in a viscoelastic material depends upon the entire history of the singular asymptotic stress and strain fields at the crack tip during the time the tip is advancing. This energy flux, referred to previously as the energy release rate and hereafter denoted by G , is difficult to calculate from the singular fields. For this reason it is convenient to introduce a Barenblatt type failure zone behind the crack tip in order to cancel the singular asymptotic fields in front of the crack. Adopting the same notation as in [2] and [3], the applied external tractions, $\sigma_{yy}^-(x,0) = f(x)$, will now be denoted by $\sigma_e^-(x)$ with the cohesive failure stresses $\sigma_f^-(x)$ acting in a failure zone of length a_f . As pointed out in [2] what results from incorporating a failure zone behind the crack tip is that the energy flux into the crack tip may be expressed as

$$G = - \int_{-a_f}^0 \sigma_f^-(x) u_{,x}^-(x) dx \quad (12)$$

where now $u(x) = u_3(x, h^+) - u_3(x, h^-)$ is the relative crack face displacement corresponding to the combined loading $\sigma_e^- + \sigma_f^-$.

As in the previous studies, the external load σ_e^- and failure zone stresses, σ_f^- , will be assumed to have the forms

$$\sigma_e^-(x) = L_e e^{x/a_e}, \quad \sigma_f^-(x) = -L_f e^{x/a_f}, \quad -\infty < x < 0. \quad (13)$$

For $a_f/a_e \ll 1$ the essential features of the Barenblatt model are

satisfied by the assumptions (13), namely a set of cohesive stresses and associated length scale a_f and a length scale a_e associated with the applied load σ_e^- such that σ_f^- cancels the singular stresses produced by σ_e^- . When σ_f^- and σ_e^- are given by (13), (12) is replaced by

$$G = - \int_{-\infty}^0 \sigma_f^-(x) u_{,x}^-(x) dx. \quad (14)$$

Applying the Parseval formula for the Fourier transform, (14) may be written as

$$G = - \int_{-\infty}^{\infty} \check{\sigma}_f^-(p) \hat{u}_{,x}^-(p) dp \quad (15)$$

where \check{f} denotes the inverse Fourier transform

$$\check{f}(p) = \frac{1}{2\pi} \int_{-\infty}^{\infty} f(x) e^{-ixp} dx.$$

From (13) it follows that

$$\hat{\sigma}_f^-(p) = \frac{-a_f L_f}{(1+ia_f p)}, \quad \check{\sigma}_f^-(p) = \frac{-a_f L_f}{2\pi(1-ia_f p)} \quad (16)$$

with similar expressions for $\hat{\sigma}_e^-$ and $\check{\sigma}_e^-$. Since $\hat{u}_{,x}^-$ has an analytic extension to the lower half-plane given by $F^-(z)$ and $\check{\sigma}_f^-$ has a meromorphic extension to the lower half-plane with a simple pole at $-i/a_f$, the integral in (15) may be evaluated using residues. This calculation yields

$$G = L_f F^-(-i/a_f).$$

Utilizing the general method for evaluating $F^-(-i/a_f)$ presented in [3] one finds

$$G = \frac{(a_f - a_e)}{(a_f + a_e)} \frac{L_e^2}{2} \frac{X^-(-i/a_f)X^+(i/a_f)}{[X^+(i/a_e)]^2} \quad (17)$$

where X^\pm are defined by (8). A convenient factorization of G which allows for comparisons between the single and two crack problems is achieved by recalling $X^\pm = X_1^\pm X_2^\pm$ and writing $G = G_1 G_2$ where

$$G_1 = \frac{(a_f - a_e)}{(a_f + a_e)} \frac{L_e^2}{2} \frac{X_1^-(-i/a_f)X_1^+(i/a_f)}{[X_1^+(i/a_e)]^2}$$

and

$$G_2 = \frac{X_2^-(-i/a_f)X_2^+(i/a_f)}{[X_2^+(i/a_e)]^2} = \frac{\tilde{X}_2^-(-i/a_f)\tilde{X}_2^+(i/a_f)}{[\tilde{X}_2^+(i/a_e)]^2} \quad (18)$$

It was shown in [1] that two cases arise naturally in constructing X_1^\pm : $0 \leq v < C^*$ and $C^* < v < C$ where $C^* = (\mu(\infty)/\rho)^{1/2}$ and $C = (\mu(0)/\rho)^{1/2}$ are the elastic shear wave speeds corresponding to the equilibrium and glassy values of the shear modulus $\mu(t)$. If a characteristic time scale, τ , is introduced and the shear modulus given in the form

$$\mu(t) = \mu_\infty m(t/\tau)$$

where $m(s)$ is a nondimensional function of s with $\lim_{s \rightarrow \infty} m(s) = 1$ and $\mu_\infty = \lim_{t \rightarrow \infty} \mu(t)$, then $\gamma_1(p) = (1 - \rho v^2 / \mu_\infty m(iV\tau p))^{1/2}$ and from [2] it then follows that G_1 may be expressed as

$$G = \left(\frac{1-\varepsilon}{1+\varepsilon}\right) \left(\frac{a_e L_e^2}{2u_\infty}\right) \left[\frac{1 - (\varepsilon\beta)^2}{1 - \gamma^2 / \overline{m}(\frac{\alpha\gamma}{\varepsilon})}\right]^{1/2}. \quad (19)$$

In (19) the following nondimensional parameters have been introduced

$$\alpha \equiv C^* \tau / a_e, \quad \beta \equiv q_0 a_e, \quad \gamma \equiv V / C^*, \quad \varepsilon \equiv a_f / a_e$$

and $q_0 = 0$ for $0 \leq V < C^*$ while for $C^* < V < C$, q_0 satisfies

$$V q_0 \int_0^\infty (\mu(t) / \mu(0)) e^{-q_0 V t} dt = (V/C)^2.$$

Now write $G_2 = 2\tilde{G}_2$ so that from (18) and (9) there results

$$\log(\tilde{G}_2) = \frac{1}{2\pi i} \int_{-\infty}^{\infty} \log(\tilde{G}_2(s)) \left[\frac{1}{s-i/a_f} + \frac{1}{s+i/a_f} - \frac{2}{s-i/a_e} \right] ds.$$

Making the substitution $s = p/a_e$ and introducing the nondimensional parameter $h/a_e = \delta$ one finds

$$\begin{aligned} \log(\tilde{G}_2) &= \frac{-1}{\pi} \int_{-\infty}^{\infty} \log \left[1 + \exp(-2|p| \delta (1 - \gamma^2 / \overline{m}(\frac{iV\tau p}{a_e}))^{1/2}) \right] \left[\frac{1}{p^2+1} + \frac{ip(\varepsilon^2-1)}{(p^2+1)(1+(\varepsilon p)^2)} \right] dp. \\ &= \frac{2}{\pi} \int_0^\infty h(p) dp \end{aligned} \quad (20)$$

where

$$h(p) = \frac{\tan^{-1}(v/u)p(\varepsilon^2-1)}{(1+p^2)(1+(\varepsilon p)^2)} - \frac{\log \sqrt{u^2 + v^2}}{p^2+1}$$

$$u = 1 + e^x \cos y, \quad v = e^x \sin y$$

$$x = -\sqrt{2} p \delta (\sqrt{s^2 + t^2} + s)^{1/2}, \quad y = -\sqrt{2} p \delta (\sqrt{s^2 + t^2} - s)^{1/2}$$

$$\text{and} \quad \left(1 - \gamma^2 / \bar{m} \left(\frac{i \sqrt{t} p}{a_e}\right)\right)^{1/2} = (s + it)^{1/2}. \quad (21)$$

Note that the effects of the crack separation distance, h , are contained in the term G_2 while G_1 , which was computed in [2], represents one half the energy flux into the crack tip for the single crack problem. It is easy to verify that as $h \rightarrow \infty$, $G \rightarrow 2G_1$, the ERR for the single crack problem, and as $h \rightarrow 0$, the work input into the crack tip is reduced by one half since $G \rightarrow G_1$.

The methods used to evaluate (14) when applied to (11) show that the stress intensity factor may be expressed as

$$\begin{aligned} K &= \frac{-L_e |\tilde{G}_1(\infty)|^{1/2}}{\sqrt{\pi}} \frac{1}{\tilde{X}_1^+(i/a_e)} \frac{1}{\tilde{X}_2^+(i/a_e)} \\ &= K_1 \frac{1}{\tilde{X}_2^+(i/a_e)} \end{aligned}$$

where K_1 is the SIF for the single crack problem found in [1]. The same reasoning leading to (20) yields

$$\log (\tilde{X}_2^+(i/a_e)) = \frac{1}{\pi} \int_0^\infty k(p) dp \quad (21)$$

where

$$k(p) = \frac{1}{(1+p^2)} (\log \sqrt{u^2 + v^2} + p \tan^{-1}(v/u))$$

with u and v defined as above. Again it is easily verified that as $h \rightarrow \infty$, $K \rightarrow K_1$.

This section concludes with the observation that the corresponding results for the elastic problem are easily recovered from the above calculations by setting $\alpha = 0$ and $n = 0$, in which case $C = C^*$ and $0 \leq \gamma < 1$. In the next section the qualitative behavior of the ERR is illustrated by numerically evaluating G for special cases of the shear modulus.

4. Numerical Examples

G will now be computed for the special cases of a standard linear solid and power-law material. First considered is the standard linear solid, which is modeled by a shear modulus of the form

$$\begin{aligned}\mu(t) &= \mu_{\infty}(1 + \eta e^{-t/\tau}) \\ &= \mu_{\infty}m(t/\tau).\end{aligned}$$

In this case $\bar{m}(w) = (1+w(1+\eta))/(1+w)$ and s and t defined in (21) are given by

$$\begin{aligned}s &= \frac{(1-\gamma^2) + (\rho\alpha\gamma)^2(1+\eta)(1+\eta-\gamma^2)}{1 + (\rho\alpha\gamma(1+\eta))^2} \\ t &= \frac{\rho\alpha\gamma^3\eta}{1 + (\rho\alpha\gamma(1+\eta))^2}\end{aligned}$$

For the standard linear solid restriction $0 < V < C$ corresponds to $0 \leq \gamma^2 < 1+\eta$.

In the case of a power law material the shear modulus is assumed to have the form

$$\begin{aligned}\mu(t) &= \mu_{\infty}(1 + (t/\tau)^{-n}), \quad 0 < n < 1 \\ &= \mu_{\infty}m(t/\tau).\end{aligned}$$

Now $\bar{m}(w) = 1 + \Gamma(1-n)w^n$ and if $\alpha_1 = \alpha[\Gamma(1-n)]^{1/n}$, s and t are given by

$$s = 1 - \gamma^2 \left\{ \frac{1 + (p\alpha_1 \gamma)^n \cos\left(\frac{n\pi}{2}\right)}{1 + 2(p\alpha_1 \gamma)^n \cos\left(\frac{n\pi}{2}\right) + (p\alpha_1 \gamma)^{2n}} \right\}$$

$$t = \frac{\gamma^2 (p\alpha_1 \gamma)^n \sin\left(\frac{n\pi}{2}\right)}{1 + 2(p\alpha_1 \gamma)^n \cos\left(\frac{n\pi}{2}\right) + (p\alpha_1 \gamma)^{2n}}$$

In this case the glassy wave speed C is infinite so that $0 \leq \gamma < \infty$.

Since a formula for G_1 is given in [2], to calculate G it suffices to numerically integrate (20). Certain care must be exercised in performing the necessary integrations as the integrand $h(p)$ may display a steep cusp near the origin along with severe oscillation for certain ranges of the parameters considered. Adaptive Gaussian integration techniques were utilized in obtaining the following results.

In Figure 1, G_2 for the standard linear solid is plotted against $\log \gamma$ when $\gamma < 1$ and against $\log\left(\frac{(\sqrt{n+1} - 1)}{(\sqrt{n+1} - \gamma)}\right)$ for $1 < \gamma < \sqrt{1+n}$ with $\delta = 1$, $n = 10$, $\epsilon = .01$, and $\alpha = .1, 1, 10, 100$. One explanation for these results is suggested by noting that $\delta/\alpha = h/c^*t$ so that small values of α correspond to a crack separation distance that is large compared to the distance a signal travels at the speed of an equilibrium shear wave during a characteristic unit of time. Figure 1 illustrates that when δ/α is large, the power input into the crack tip approaches that corresponding to the single crack problem. As δ/α becomes small, this effect occurs only at crack propagation speeds that approach the glassy shear wave speed. The normalized ERR for the standard linear solid, g , defined by

$$G = \left(\frac{1-\epsilon}{1+\epsilon}\right) \left(\frac{a_e L_e^2}{2\mu_\infty}\right) g$$

is graphed in Figure 2. The behavior of g is qualitatively similar to that for the single crack problem and the appropriate comments in [2] apply here. The corresponding results for the power law model appear in Figures 3 and 4. The only significant difference is that in Figure 3 G_2 always attains the value corresponding to the single crack problem. This is explained by the fact that for the power-law model, the glassy shear wave speed is infinite. Thus this model allows sufficiently large crack propagation speeds to overcome the effect of δ/α , which may be regarded as a measure of the influence that one crack tip has on the other.

The remaining figures apply to a standard linear solid. (The corresponding graphs for the power-law model are qualitatively similar.) In Figures 5 and 6 G_2 is graphed versus $\log(\delta)$ when $\epsilon = .01$, $\alpha = .1, 1, 10, 100$ and $\gamma = 3.3$ and 1 , respectively, corresponding to crack propagation speeds near the glassy and equilibrium values. G_2 is seen to be a monotonic increasing function of the crack separation distance. Material effects, corresponding to the various values of α , are seen to have a greater effect upon the ERR at a large crack propagation speed, as in Figure 5, than at the slower crack speed displayed in Figure 6. The previous comments concerning δ/α are consistent with the behavior of G_2 illustrated in these figures. Figures 7 and 8 display G_2 versus $\log(\delta)$ for varying crack speeds and $\alpha = .1$ and 100 , respectively. These figures show that the ERR is more sensitive to changes in crack propagation speeds and crack separation distances at smaller values of α . The results of Figure 7 show that except for a small range of slow crack speeds, the influence of the two cracks upon the ERR decreases with increasing crack

propagation speed. When α is large, as in Figure 8, the reduction in the work input into the crack tip due to the presence of two cracks is only overcome at large crack separation distances. Figure 9 illustrates the influence of viscoelasticity in conjunction with crack separation distance. As might be expected, as viscous effects increase, G tends to the value of the single crack problem.

In evaluating (22) it was found that the qualitative behavior of $1/\tilde{X}_2^+(i/a_e)$ is similar to that of G_2 with the SIF, K , being similar to the single crack SIF presented in [2]. For this reason the normalized SIF, $k = \frac{-K}{L_e} \sqrt{\frac{\pi}{a_e}}$, which with the results of [2] is seen to be $k = \frac{1}{\sqrt{1+\beta}} \frac{1}{\tilde{X}_2^+(i/a_e)}$, is plotted only for the standard linear solid.

References

- [1] J. R. Walton, On the Steady-State Propagation of an Anti-Plane Shear Crack in an Infinite General Linearly Viscoelastic Body, Quarterly of Applied Mathematics 40 (1982) 37-52.
- [2] J. R. Walton, The Dynamic Energy Release Rate for a Steadily Propagating Anti-Plane Shear Crack in a Linearly Viscoelastic Body, Report MM 4867-86-3, Mechanics and Materials Center, Texas A&M University, (1986).
- [3] L. Schovanec and J. R. Walton, The Energy Release Rate for a Quasi-Static Mode I Crack in a Non-homogeneous Linearly Viscoelastic Body, Submitted for publication.

Figure Captions

- Figure 1. G_2 versus $\log(\gamma)$ for $\gamma < 1$ and $\log((\sqrt{\eta+1} - 1)/(\sqrt{\eta+1} - \gamma))$ for $1 < \gamma < \sqrt{\eta+1}$ for a standard linear solid with $\delta = 1$, $\eta = 10$, $\epsilon = .01$, and $\alpha = .1$ (—), 1.0 (— — — —), 10 (— · —), 100 (— —).
- Figure 2. g versus $\log(\gamma)$ for $0 < \gamma < 1$ and $\log((\sqrt{\eta+1}-1)/(\sqrt{\eta+1}-\gamma))$ for $1 < \gamma < \sqrt{\eta+1}$ for a standard linear solid with $\delta = 1$, $\eta = 10$, $\epsilon = .01$, and $\alpha = .1$ (—), 1.0 (— — — —), 10 (— · —), 100 (— —).
- Figure 3. G_2 versus $\log(\gamma)$ for a power-law material with $\delta = 1$, $n = .3$, $\epsilon = .01$, and $\alpha = .1$ (—), 1.0 (— — — —), 10 (— · —), 100 (— —).
- Figure 4. g versus $\log \gamma$ for a power-law material with $\delta = 1$, $n = .3$, $\epsilon = .01$, and $\alpha = .1$ (—), 1.0 (— — — —), 10 (— · —), 100 (— —).
- Figure 5. G_2 versus $\log(\delta)$ for a standard linear solid with $\eta = 10$, $\epsilon = .01$, $\gamma = 3.3$, and $\alpha = .1$ (—), 1.0 (— — — —), 10 (— · —), 100 (— —).
- Figure 6. G_2 versus $\log(\delta)$ for a standard linear solid with $\eta = 10$, $\epsilon = .01$, $\gamma = 1.0$, and $\alpha = .1$ (—), 1.0 (— — — —), 10 (— · —), 100 (— —).
- Figure 7. G_2 versus $\log(\delta)$ for a standard linear solid with $\eta = 10$, $\epsilon = .01$, $\alpha = .1$, and $\gamma = .1$ (—), 1.0 (— — — —), 10 (— · —), 100 (— —).

Figure 8. G_2 versus $\log(\delta)$ for a standard linear solid with $\eta = 10$, $\varepsilon = .01$, $\alpha = 100$, and $\gamma = .1$ (—), 1.0 (- - -), 10 (- · -), 100 (— —).

Figure 9. G_2 versus $\log(\delta)$ for a standard linear solid with $\varepsilon = .01$, $\alpha = 1$, and $\gamma = 1$, and $\eta = .1$ (—), 1.0 (- - - -), 10 (- · -), 100 (- -).

Figure 10. The normalized SIF k versus $\gamma/(\eta+1)^{1/2}$ for a standard linear solid with $\delta = 1$, $\eta = 10$, and $\alpha = .1$ (—), 1.0 (- - - -), 10.0 (- · -).

Figure 1.

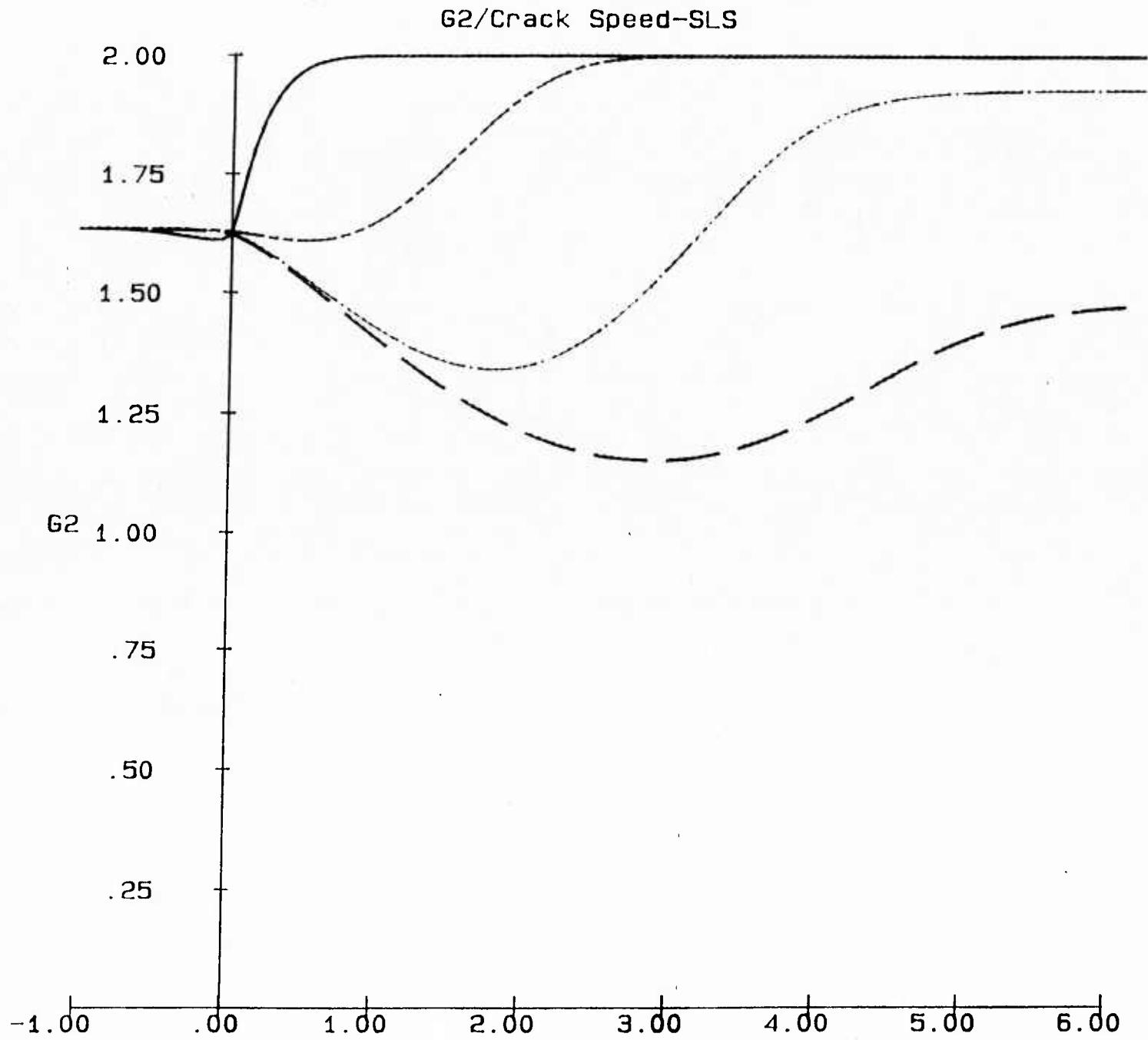


Figure 1

Figure 2.

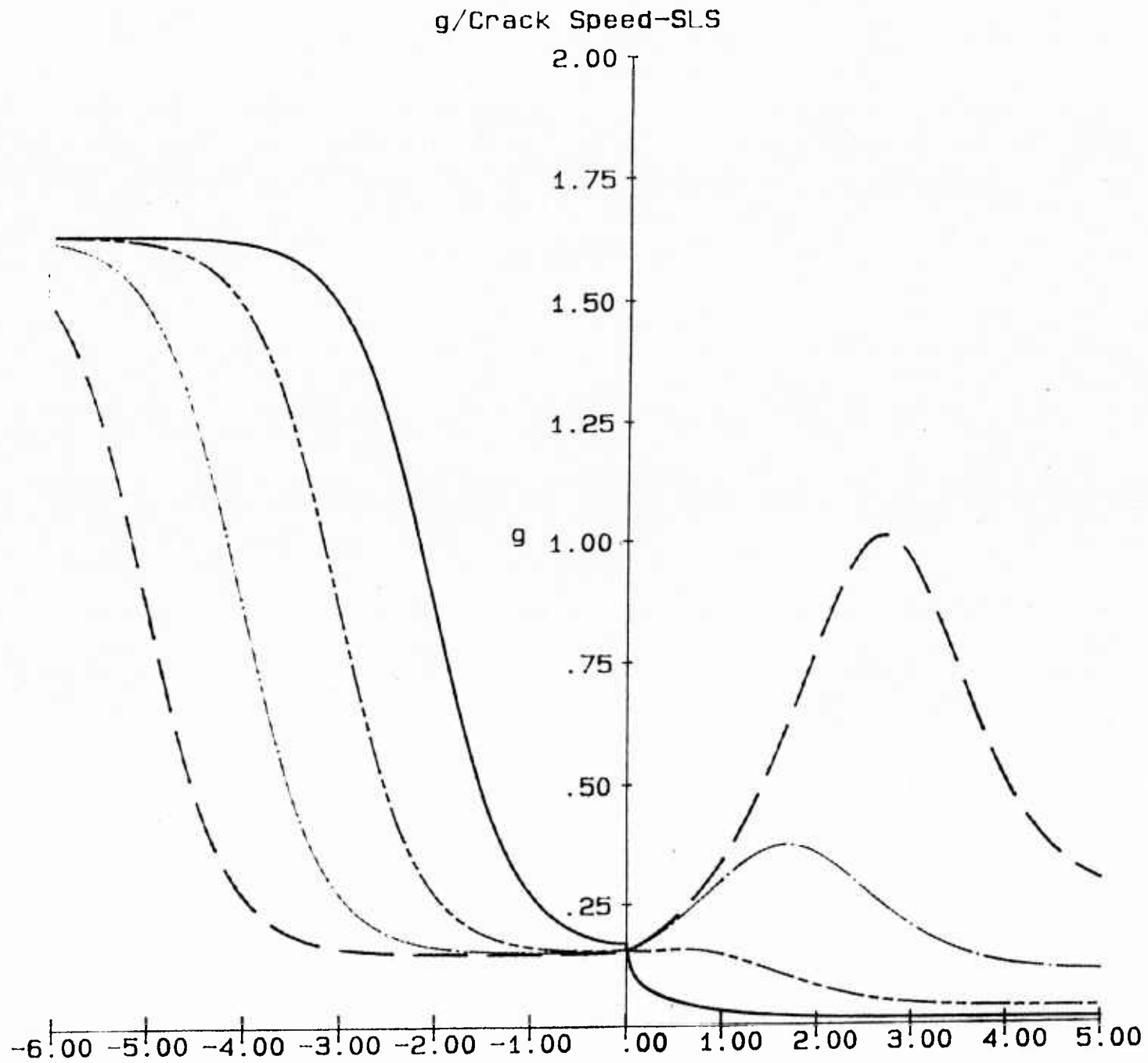


Figure 2

Figure 3.

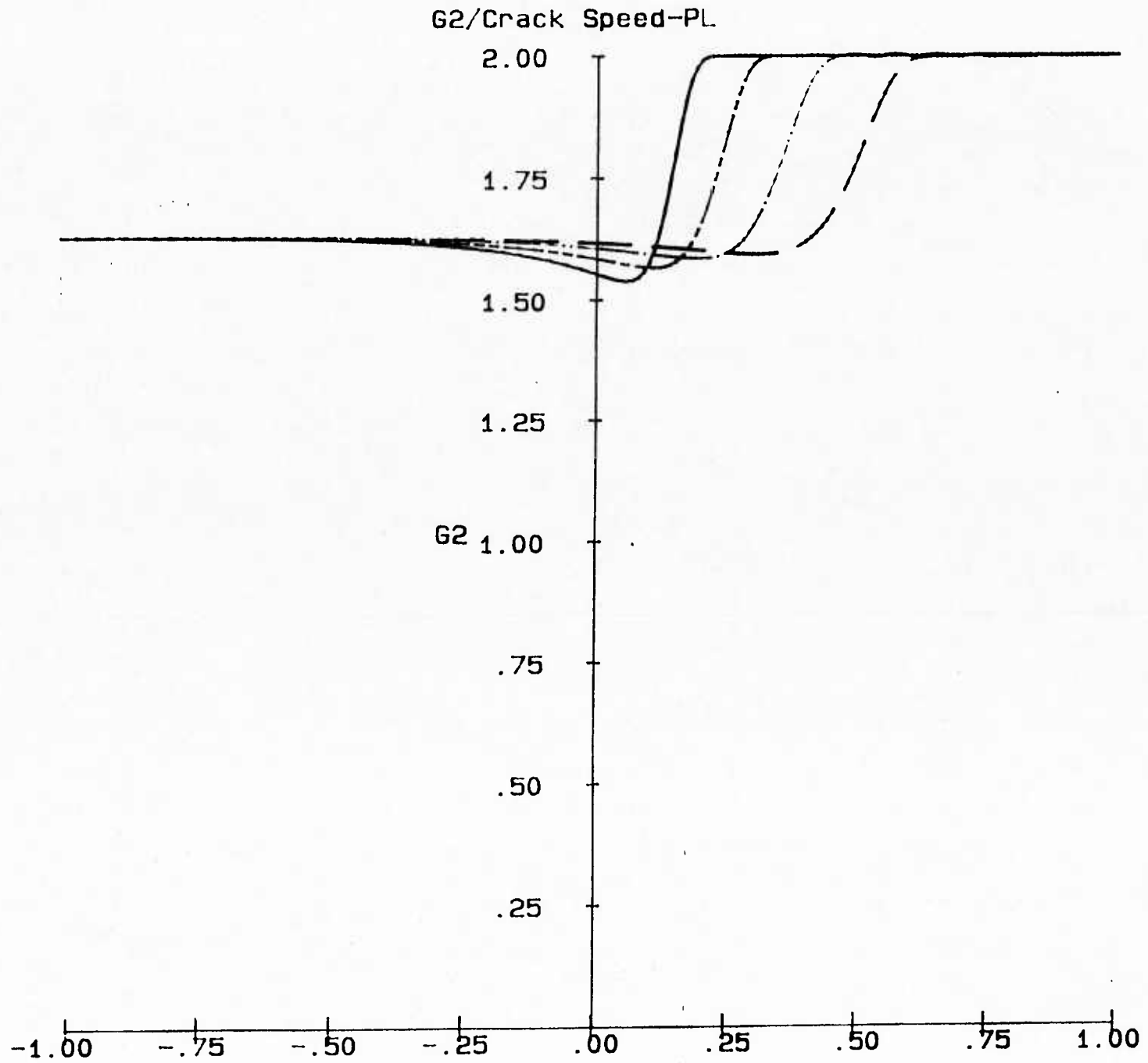


Figure 3

Figure 4.

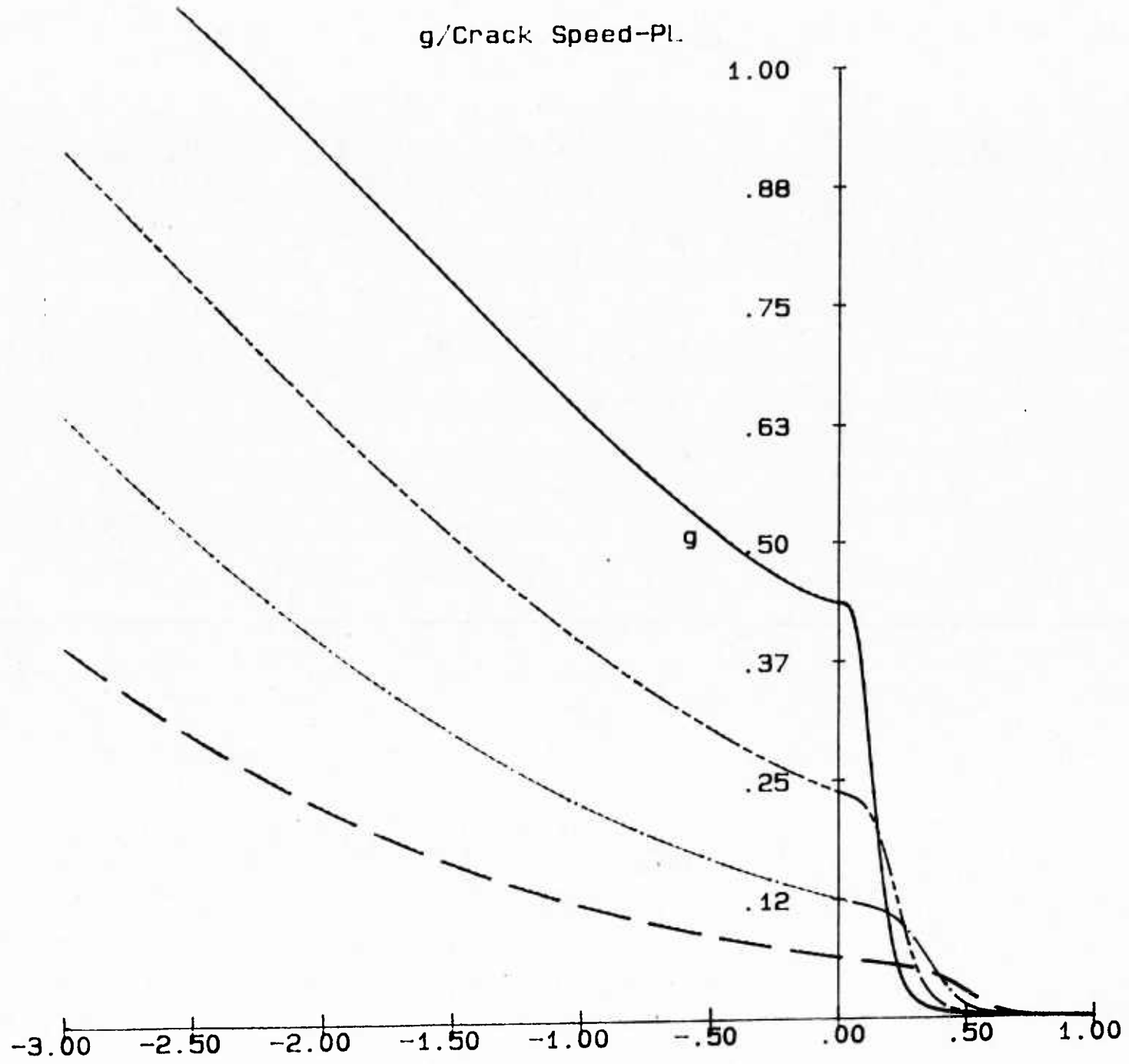


Figure 4

Figure 5.

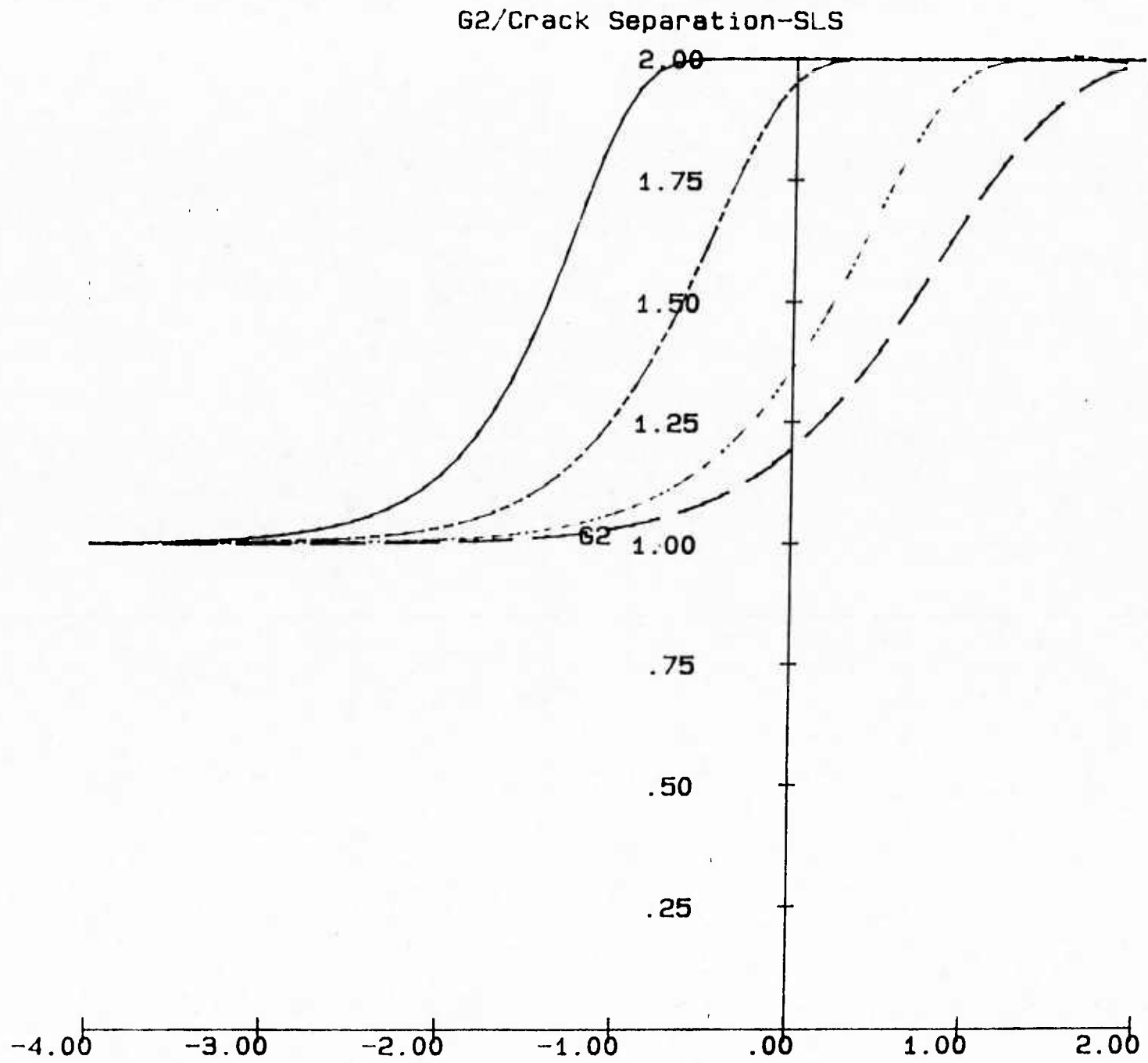


Figure 5

Figure 6.

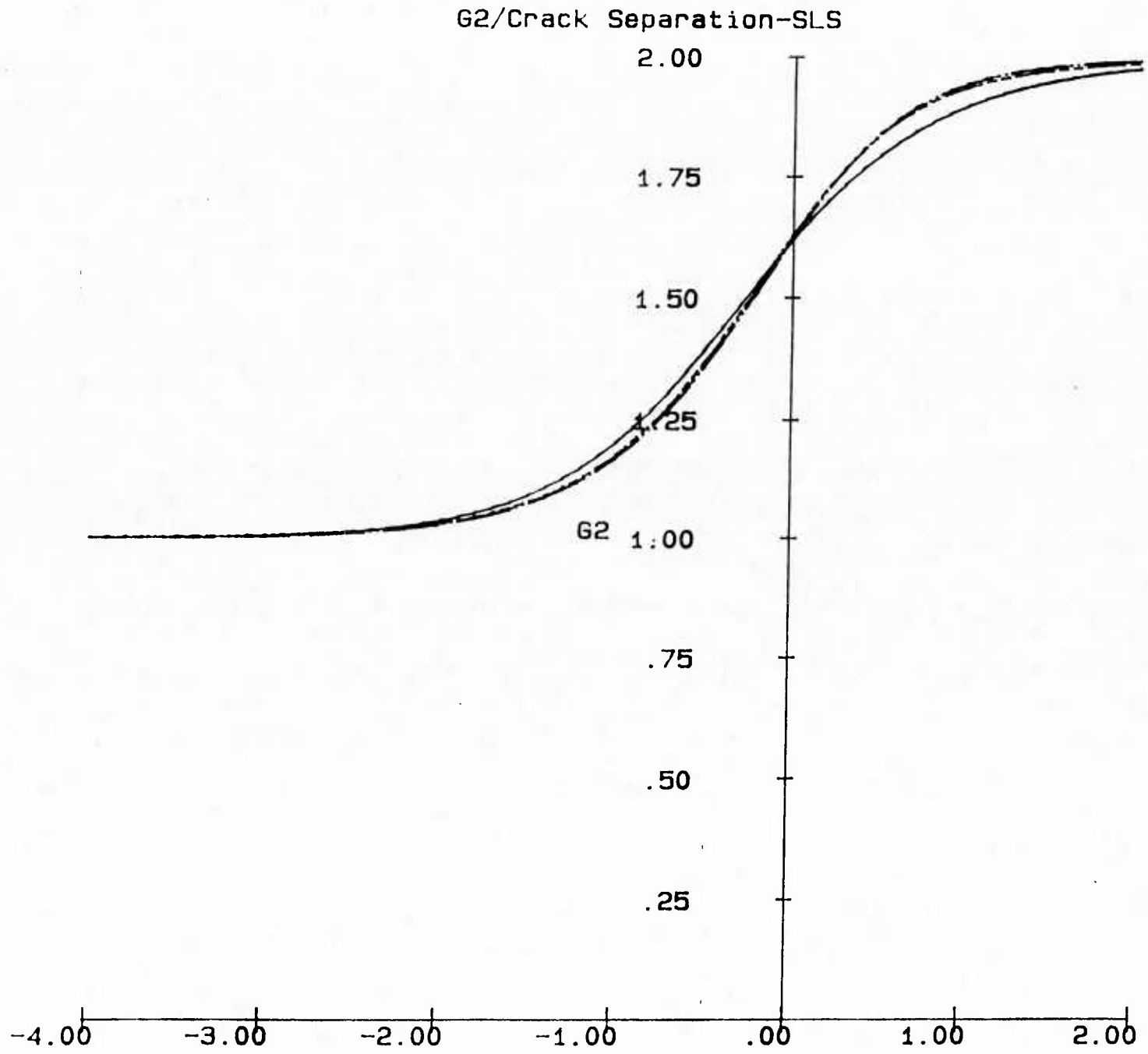


Figure 6

Figure 7.

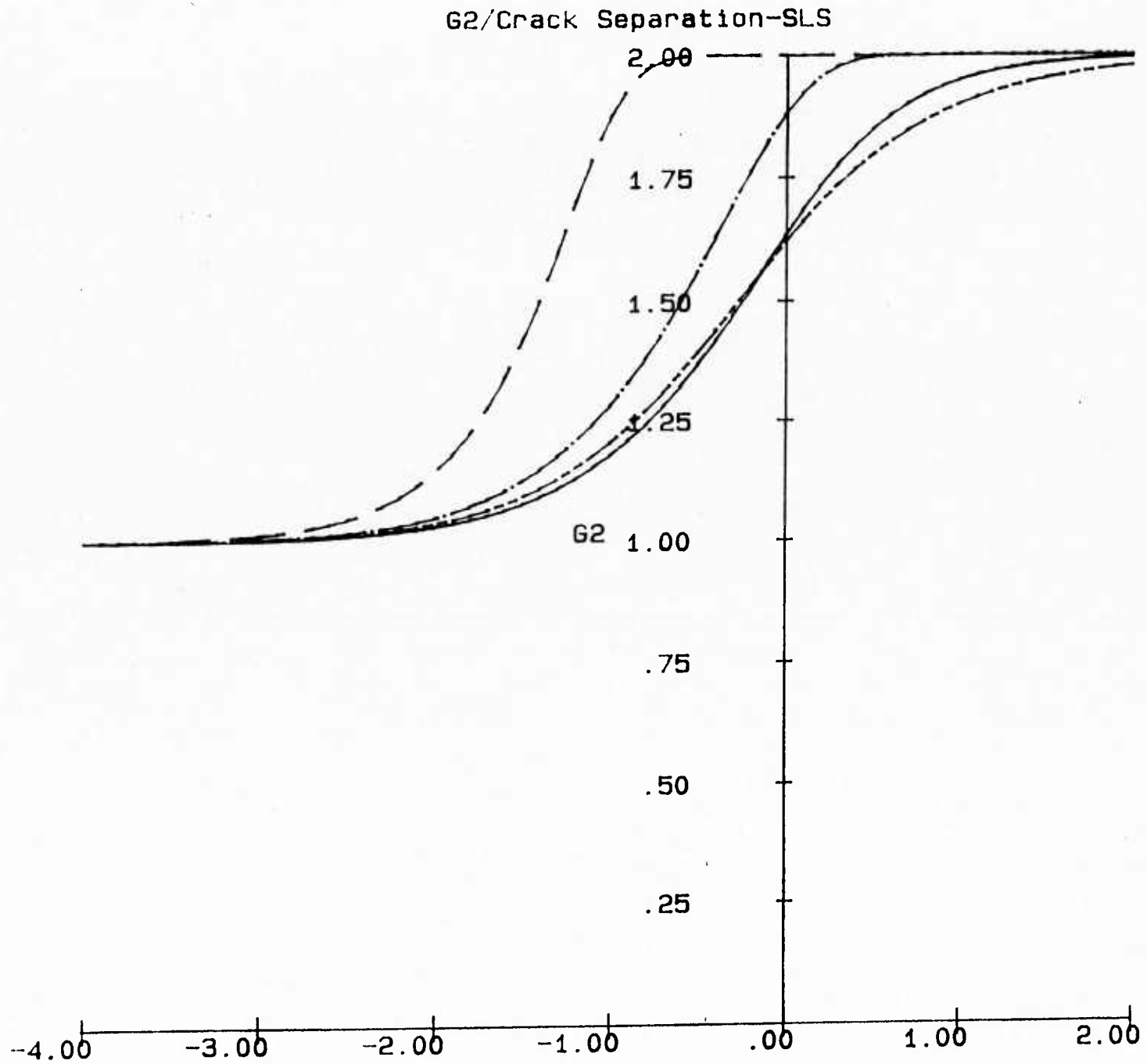


Figure 7

Figure 8.

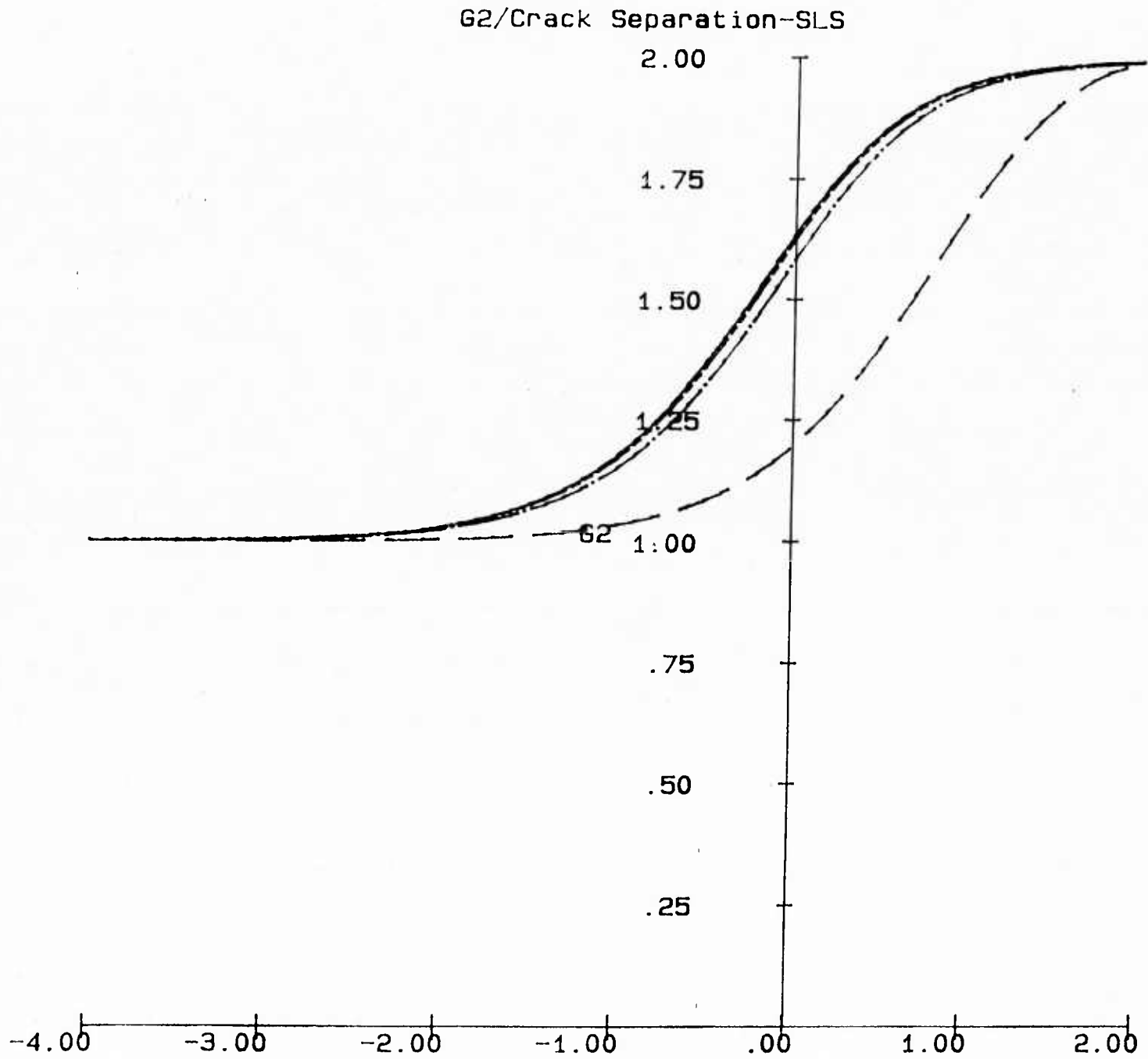


Figure 8

Figure 9.

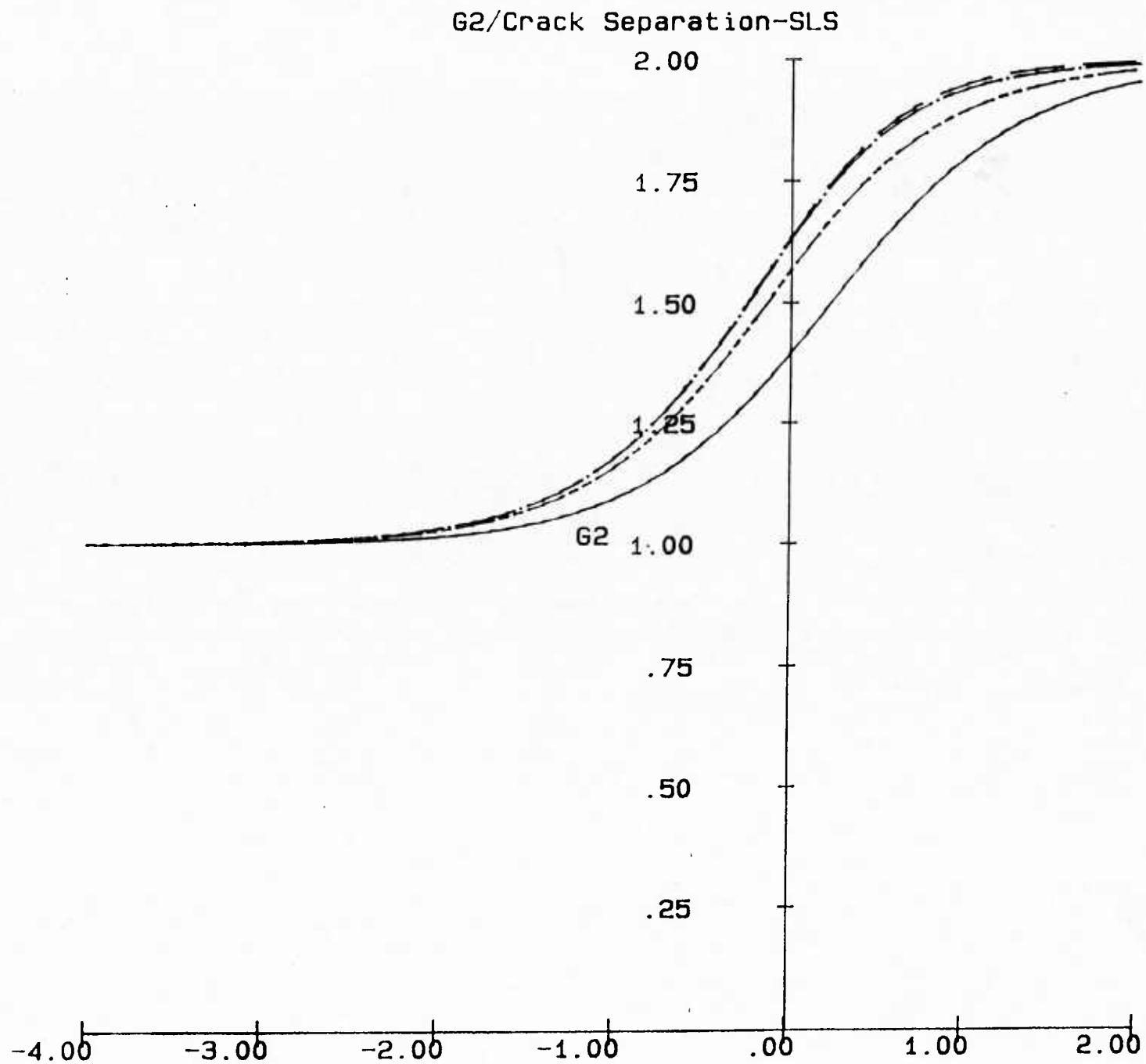


Figure 9

Figure 10.

SIF/Crack Speed-SLS

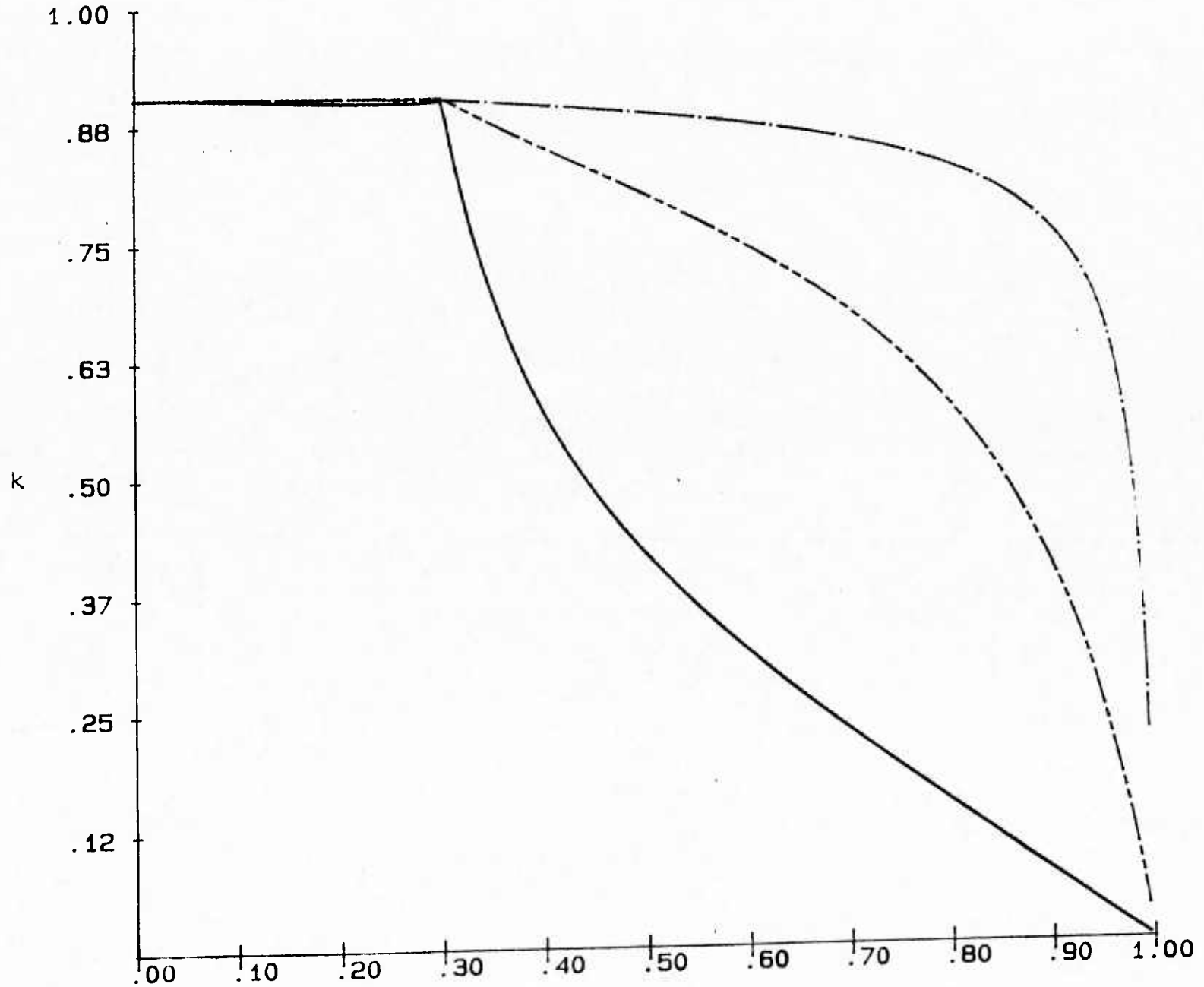


Figure 10